Chem Rev Lett 8 (2025) 1258-1268

Research Article

Chemical Review and Letters

journal homepage: www.chemrevlett.com

ISSN (online): 2645-4947 (print) 2676-7279

DFT investigation of aflatoxin B1 adsorption on vacancy-defective graphene: Electronic properties and sensing potential

Mohammad Haghgu[1], Zahra Rostami[1, *], Azizbek Mengboev[2]

[1]*Department of Chemistry, Payame Noor University (PNU), Tehran, Iran.*

[2]*Faculty of Pedagogy and Social-Humanitarian Sciences, Interfaculty Department of Foreign Languages, Termez University of Economics and Service, P. O. Box: 190111, Termez, Uzbekistan.*

ARTICLE INFO

Article history:
Received 31 August 2025
Received in revised form 12 November 2025
Accepted 13 November 2025

Keywords:
Aflatoxin B1
Sensor
Perfect
Single- and double- vacancy defective graphenes
Density functional theory
AIM analysis

ABSTRACT

Aflatoxins (AFs) are highly toxic compounds that pose substantial health risks, with Aflatoxin B1 (AFB1) being a highly toxic mycotoxin with severe health implications, necessitating rapid and sensitive detection methods. This study aims to investigate the potential of defect-engineered graphene nanosheets as electronic sensors for AFB1 detection. Using density functional theory (DFT), the adsorption behavior of AFB1 on perfect graphene (PG), single-vacancy graphene (SVG), and double-vacancy graphene (DVG) was systematically analyzed. The results revealed weak physisorption on PG, with minimal influence on its electronic properties, whereas vacancy defects introduce reactive sites that markedly enhance adsorption strength and sensor response. In SVG, adsorption lowers the energy gap from 0.81 eV to 0.54 eV and decreases the work function from 3.57 eV to 3.53 eV, leading to increased conductivity and field emission current. The Atoms in Molecules (AIM) analysis indicates that the interactions are predominantly van der Waals in nature, confirming a physisorption-dominated mechanism. These findings demonstrate that single-vacancy defective graphene offers superior sensitivity and electronic modulation, underscoring its promise as an efficient nanosensor for AFB1 detection and highlighting the critical role of defect engineering in graphene-based sensor design.

1. Introduction

Aflatoxins (AFs) are among the most harmful mycotoxins produced by fungi such as the *Aspergillus* species. These filamentous fungi have a widespread distribution and are prevalent contaminants of food and various agricultural commodities, including grains, corn, cotton, walnuts, peanuts, and others [1–3]. Aflatoxins are highly toxic, with the main types being B_1, B_2, G_1, and G_2; among these, Aflatoxin B1(AFB1) is considered the most toxic. Aflatoxins can pose health risks to humans via respiratory, mucosal, or dermal routes [4]. Since public health largely depends on food production standards, and because contaminated food and agricultural products can endanger health and lead to fatal diseases, it is crucial to test these products for aflatoxin contamination prior to consumption [5].

Various detection methods have been developed to identify aflatoxin contamination in grains, and numerous sensors have been designed to detect low levels of these toxins [6]. However, there remains a significant need for rapid, sensitive, and specific techniques capable of detecting aflatoxins at trace levels.

In recent years, the use of graphene and carbon nanotubes has garnered particular attention in sensor technology, owing to their exceptional properties that render them highly suitable for sensor design [7]. Graphene is one of the most remarkable materials available today, and its synthesis has generated considerable excitement among scientists [8,9]. Since 2004, its applications have expanded across numerous fields, owing to its unique features, such as a two-dimensional conjugated structure with a thickness of a single atom, excellent stability at room temperature, high charge transfer capabilities, and a large specific surface area [10–13].

The high electrical conductivity of graphene ensures minimal signal disturbance when used as a chemical sensor, making it an ideal candidate for gas and vapor

---

* Corresponding author E-mail: Rostami@pnu.ac.ir

https://doi.org/10.22034/crl.2025.544347.1683

detection. Consequently, extensive research has been conducted in the field of graphene-based gas/vapor sensors, with the number of published articles on this topic increasing rapidly since 2007 [14–18]. However, because perfect graphene exhibits weak interactions with most chemical compounds, various methods have been employed to address this challenge, including heteroatom doping and the creation of defects [19]. Previous density functional theory (DFT) studies have shown that introducing defects in graphene enhances its adsorption capacity, thereby improving its chemical sensing performance [11–22].

Removing or displacing carbon atoms from the graphene plane results in the breaking of covalently bonded electron pairs. The presence of dangling-bond carbon atoms imparts new physical and chemical properties to graphene materials, thereby broadening their potential applications. Defects in graphene mainly fall into two categories: point defects and one-dimensional (1D) defects. Vacancies are among the most common point defects, and their presence increases the sensitivity of graphene while enhancing the adsorption stability of gas molecules on its surface. Graphene is an ideal platform for studying defects because its two-dimensional structure allows the easy addition, removal, and movement of carbon atoms. Notably, a carbon vacancy defect can induce magnetism by breaking the symmetry of otherwise nonmagnetic graphene. Additionally, the introduction of defects causes shifts in the energy band structure, often leading to the creation of a bandgap at the Fermi level [23]. Moreover, vacancy sites exhibit high reactivity during interactions with atoms or molecules, making them particularly significant in adsorption processes [24].

In recent years, computational chemistry has emerged as a powerful tool for designing gas and vapor sensors [25–29]. However, to the best of our knowledge, computational studies focusing on graphene-based sensors for aflatoxin detection remain limited. Therefore, this research investigates the interaction of AFB_1 with perfect graphene (PG), single-vacancy defective graphene (SVG), and double-vacancy defective graphene (DVG) sheets using DFT calculations, aiming to evaluate their potential as nanosensor materials for AFB_1 detection. The novelty of this work lies in applying DFT, together with AIM and NBO analyses, to systematically investigate Aflatoxin B1 interactions with various vacancy-defective graphene sites and to correlate adsorption geometries with distinct electronic structure signatures (band gap modulation and DOS features) relevant for sensing.

2. Computational Methods

All quantum chemical calculations were performed using the Gaussian09 software package [30]. Geometry optimizations were carried out at the B3LYP/6-31g(d) level of theory, which has been shown to provide a reliable balance between computational efficiency and accuracy in describing the structural, electronic, and optical properties of nanostructured and carbon-based systems [31–34]. Based on the optimized geometries, Atoms in Molecules (AIM), Natural Bond Orbital (NBO), and Density of States (DOS) analyses were performed at the same level of theory. The AIM analyses were conducted using the Multiwfn (version 3.8) program on wavefunctions obtained from single-point calculations, while NBO analyses were performed using the built-in NBO 3.1 module of Gaussian09. DOS plots and related electronic density data were generated using the GaussSum software. All geometry optimizations were performed with the default convergence thresholds as implemented in Gaussian09 [31–34]. A review of the literature indicates that the B3LYP functional is an efficient density functional for estimating the van der Waals interactions relevant to Aflatoxin B1 adsorption, as previous benchmarks on carbon-based adsorbents and organic adsorbates have shown that it reliably describes both the electronic structure and dispersion-dominated interactions [35–41]. The adsorption energy (E_{ad}) was measured as:

$$Ead = E(complex) – E(sheet) – E(AFB1) + EBSSE \quad (1)$$

where E(complex) represents the AFB1/nanosheet complex energy, while E(AFB1) denotes the isolated AFB1 molecule energy. The counterpoise correction method was employed to estimate the basis set superposition error energy (EBSSE) [42]. The energy gap (Eg) between the HOMO and LUMO levels is expressed as:

$$Eg = ELUMO – EHOMO \quad (2)$$

3. Results and Discussion

3.1. Properties of perfect and defected graphene nanosheets

The optimized structures of SVG and DVG were investigated, and their electronic properties are illustrated in Figure 1, which also includes the perfect graphene sheet for comparison. Analysis of the DOS spectra in Figure 1 indicates that SVG exhibits the lowest energy gap, whereas DVG displays the highest (Table 1). It is likely that the formation of pseudo-pentagonal rings within DVG contributes to the enhanced stability of this structure. Additionally, the data summarized in Table 1 reveal that SVG possesses the lowest chemical hardness, thereby implying higher chemical reactivity along with superior electrical conductivity. When a periodic single vacancy is created by removing one carbon atom from the UC (defect concentration of 0.7%), a partial reconstruction of the defective SVG sheet is observed. In this process, two of the three unsaturated carbon atoms interact, resulting in a optimized C–C distance (by approximately 0.6 Å) compared to that in perfect graphene (Figure 1).

If two adjacent carbon atoms are removed from the ideal graphene sheet, forming a vacancy pair (DVG model), the interactions between the unsaturated carbon atoms lead to the formation of two five-membered rings. The optimized C–C bond length within these rings is 1.727 Å, and the reconstructed area surrounding the vacancy pair consists of an eight-membered ring [33]. The PG, SVG, and DVG models were found to be energetically stable closed-shell systems.

Consistent with previous findings, reconstruction of the carbon network has also been reported in graphene sheets and single-walled carbon nanotubes (C-SWNTs) with vacancies.

These investigations were primarily conducted using DFT within the Local Density Approximation (LDA) and Generalized Gradient Approximation (GGA) frameworks [43–47].

3.1.1. AFB1 adsorption on perfect graphene

AFB_1 molecules possess four nucleophilic sites: the –CO group (which can interact with electron-deficient vacancies), the –COO and $–OCH_3$ groups, as well as two furan rings, as illustrated in Figure 1.

To determine the most stable AFB_1/perfect graphene (AFB_1/PG) configuration, AFB_1 was positioned such that its nucleophilic groups could interact with the edge carbon atoms of the graphene sheet.

The HOMO and LUMO profiles in Figure 2 reveal that the molecular orbitals are predominantly localized on the edge carbon atoms, indicating that AFB_1 is likely to bind more strongly at these sites.

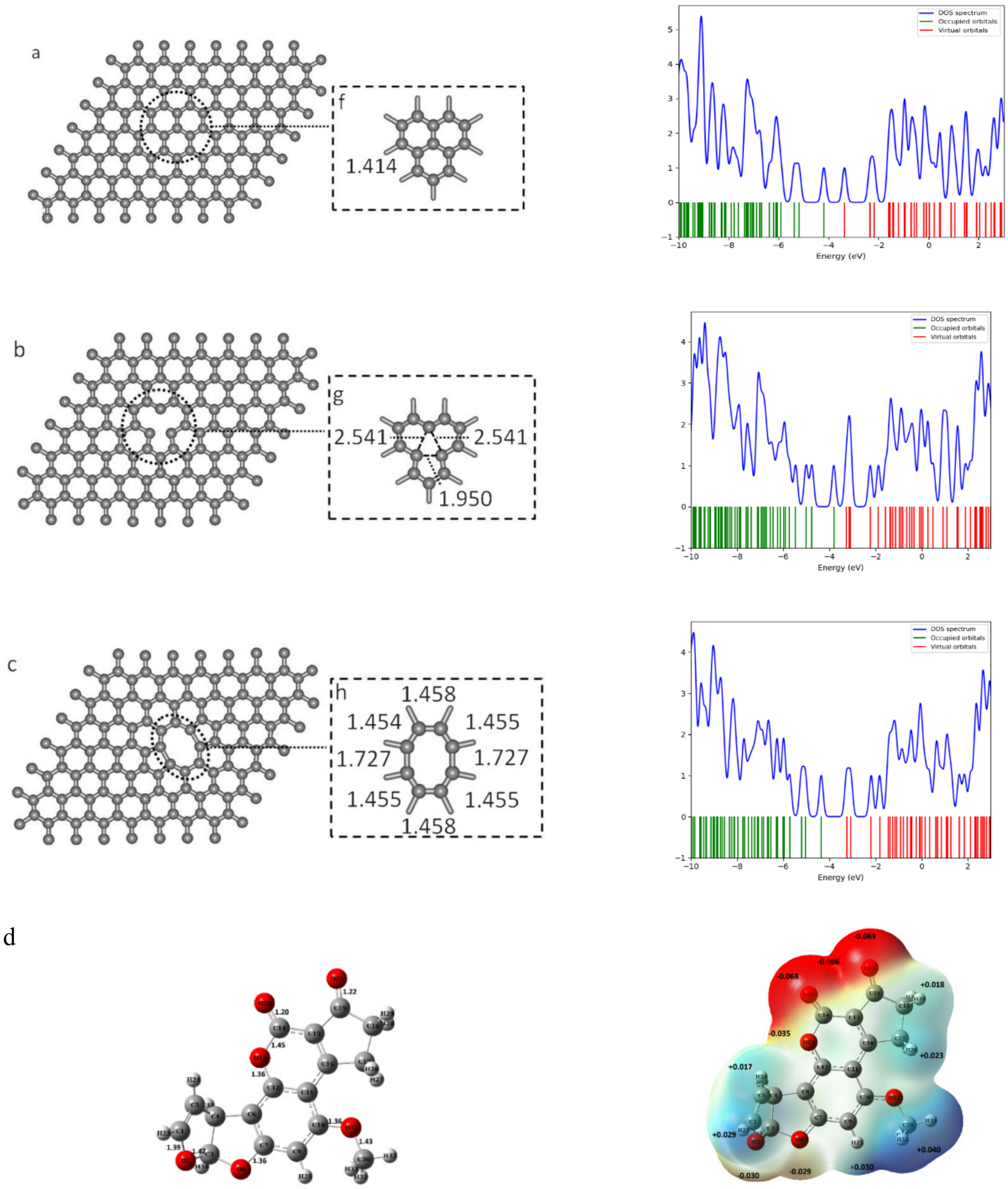

Fig. 1. Optimized structure of graphene sheets and DOS plot: (a) PG showing C–C bond distance (inset f), (b) SVG showing C–C distances around the vacancy site (inset g), (c) DVG reconstructed

Table 1: Quantum chemical descriptors for PG, SVG, DVG, and their AFB1 complexes. All calculations were performed at the B3LYP/6-31g(d) level, and values are reported in eV, except for %ΔE_{gap}, Q and %Δϕ.

System	E_{ad}	E_{HOMO}	E_{LUMO}	η	E_f	ω	A	E_g	%ΔE_g	Q	ϕ	%Δϕ
PG	-	-3.98	-3.17	0.41	-3.577	15.8	3.17	0.81	-	-	3.577	-
P1	-0.012	-3.85	-3.05	0.40	-3.449	14.8	3.05	0.80	-1.23	-0.005	3.449	-3.58
P2	-0.077	-4.10	-3.29	0.40	-3.697	16.9	3.29	0.81	0.00	-0.019	3.697	3.34
P3	-0.021	-3.87	-3.07	0.41	-3.470	14.9	3.07	0.80	-1.23	-0.002	3.470	-2.99
SVG	-	-3.81	-3.27	0.27	-3.537	23.1	3.27	0.54	-	-	3.537	-
S1	-1.049	-4.14	-3.45	0.35	-3.80	20.8	3.45	0.69	28.15	-0.017	3.80	7.29
S2	-1.026	-4.13	-3.45	0.34	-3.788	21.3	3.45	0.67	24.59	-0.019	3.788	7.07
S3	-1.196	-3.87	-2.99	0.44	-3.428	13.4	2.99	0.88	62.44	0.0073	3.428	-3.10
DVG	-	-4.14	-3.06	0.54	-3.601	11.9	3.06	1.09	-	-	3.601	-
D1	-0.563	-4.23	-3.05	0.59	-3.642	11.3	3.05	1.17	8.19	-0.04	3.642	1.13
D2	-0.554	-4.30	-3.20	0.55	-3.754	12.8	3.20	1.10	1.45	-0.024	3.754	4.23
D3	-0.833	-3.90	-2.72	0.59	-3.310	9.3	2.72	1.18	8.64	0.097	3.310	-8.10

Three adsorption configurations were considered, with AFB$_1$ binding through its –CO, –O, and –CO head groups onto the perfect graphene sheet, labeled as P1, P2, and P3, respectively (see Fig. 1 Supp. in the Supplementary Information).

The electronic parameters listed in Table 1 show that configuration P2 exhibits the highest stability, with AFB$_1$ adsorbed via its furan rings onto the PG surface (E_{ad} = −0.077 eV). In this model, both HOMO and LUMO orbitals are delocalized over the graphene sheet plane (Figure 2a), which is consistent with the expected electronic characteristics of a chemically inert material such as graphene. This delocalization makes spatial overlap between the molecular orbitals of AFB$_1$ and the HOMO/LUMO of PG highly unlikely, resulting in negligible charge transfer and weak interaction between them. According to the NBO analysis, the maximum charge transfer in the most favorable configuration (P2) was only **−0.019 e**, indicating that AFB$_1$ acts as an electron acceptor, while PG serves as an electron donor. To evaluate the sensitivity of PG toward AFB$_1$ molecules, both the energy gap and work function were calculated. Previous research has shown that the energy gap is a reliable indicator of a nanostructure's sensitivity to chemical agents, as it correlates with electrical conductivity (σ) [39]:

$$\sigma = AT^{3/2}\exp\left(\frac{-E_g}{2kT}\right) \tag{3}$$

where *K* denotes the Boltzmann constant, and *A* is a constant (electrons/m^{3}k$^{3/2}$). This correlation has been verified in numerous experimental reports [48-50]. It indicates that electrical conductivity increases sharply as the energy gap decreases, and that adsorbent molecules bind to the chemical agent within the medium. Furthermore, the effects of AFB1 on the work function and Fermi level of PG were analyzed. Both the work function and Fermi level are critical parameters for ϕ-type nanosensors. Such sensors utilize a Kelvin oscillator to measure the work function before and after adsorption [51]. Changes in the work function can alter the gate voltage and generate an electrical signal, thereby enabling detection [52]. The work function represents the minimum energy required to remove an electron from the Fermi level and is calculated using the following equation:

$$\phi = V_{el}(\infty) - E_F \tag{4}$$

where E_F denotes the Fermi level energy, and V_{el} (+∞) represents the electrostatic potential energy of electrons at large distances from the surface of the material, which is assumed to be zero. Under the condition $V_{el}(+\infty)=0$, the work function ϕ can be expressed as: $\phi=-E_F$ [53]. The Fermi level energy is given by:

$$E_F = E_{HOMO} + (E_{LUMO} - E_{HOMO})/2 \tag{5}$$

According to the classical Richardson-Dushman model, a variation in the work function value can influence the field emission current density *j* [54]:

$$j = AT^2\exp\left(\frac{-\phi}{kT}\right) \tag{6}$$

where *A* is the Richardson constant (A/m^2), and *T* represents the absolute temperature. According to Table 1, the adsorption of AFB1 caused slight changes in the HOMO, LUMO, and energy gap of PG. In configuration P1, AFB1 shifted the HOMO level from -3.98 eV to -3.85 eV and the LUMO level from -3.17 eV to -3.05 eV, resulting in a 1.23% reduction in the energy gap. Meanwhile, the Fermi level remained almost unchanged. Similar observations were made for other configurations (P2 and P3). The operating principle of an electrical sensor relies on detecting changes in electrical conductivity upon the adsorption of a chemical species. Although the adsorption of AFB1 on PG in the P1 and P3 complexes caused the largest change in the energy gap (−1.23%), the change was minimal overall, leading to only a very slight variation in the nanostructure's conductivity. Specifically, the electron population responsible for electrical conduction does not change appreciably at the reference temperature because the changes in the energy gap are negligible. Consequently, PG exhibits a limited ability to detect AFB1. To enhance the sensitivity of graphene to AFB1, the next approach involved introducing defects, such as single and double vacancies.

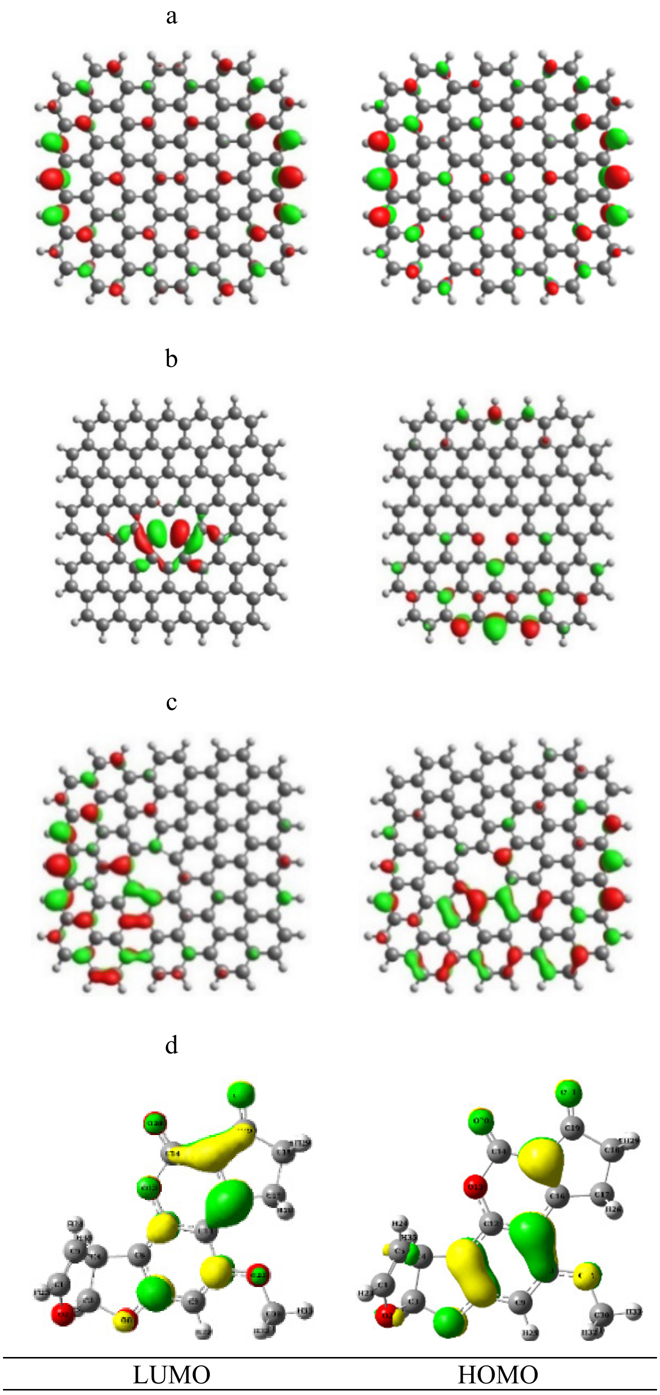

Fig. 2. LUMO and HOMO profiles: (a) PG sheet, (b) SVG sheet, (c) DVG sheet, (d) AFB1 molecule

By manipulating and adding impurities or creating such defects, the carbon network can be effectively modified, providing new opportunities for adsorption. It has been demonstrated that the presence of holes or vacancies on the surface of graphene significantly affects its electronic properties. Unsaturated carbon atoms in single- and double-vacancy graphene structures increase adsorption energy, thereby making graphene with vacancies more reactive to the presence of AFB1.

3.1.2. AFB1 adsorption onto graphene with a single vacancy

Various types of defects in graphene can be classified into intrinsic and extrinsic categories, with their dimensionality also varying [55]. A single vacancy (SV) represents the simplest defect in graphene, formed by removing one atom from the lattice. (Figure 1b illustrates the structurally optimized SVG.) Literature reports that approximately 7.5 eV is required to create a single vacancy, with the energy barrier for vacancy diffusion estimated to be around 1.3 eV. The mobility of vacancies has been observed at temperatures around 200°C [56-58]. When a carbon atom is absent, it leaves unsaturated dangling bonds, rendering the SV site highly reactive [59] . Studies have demonstrated that various atoms readily adsorb at the SV site [60–62]. The electronic parameters of SVG, shown in Table 1, indicate that defect creation alters the energy gap, reducing it from 0.81 eV to 0.54 eV, and decreasing the hardness (η) from 0.405 eV to 0.271 eV. This signifies an increase in SVG activity compared to PG. Additionally, the electrophilic index (ω) increased to 23.1 eV, indicating that SVG possesses greater nucleophilic properties than both PG and DVG. Figure 2.b depicts the HOMO and LUMO molecular orbitals for SVG. In SVG, the expansion of HOMO molecular orbital is extends (circuited cover) on the side C-C bonds, while the LUMO orbital is primarily localized on the eight carbon atoms surrounding the vacancy, which act as active sites exposed to AFB1 molecules. This orbital localization facilitates effective overlap and allows electron density transfer from AFB1 to the SVG, leading to strong AFB1–SVG interactions. To analyze the interaction mechanism, an AFB1 molecule was initially positioned above the vacancy site in the graphene plane, and the adsorption process was studied from various directions. The optimized structures of the AFB1/SVG complexes and their corresponding DOS diagrams are shown in Figure 3 (S1, S2 and S3). Based on Table 1, configuration S3 exhibited the highest structural stability, where AFB1 adsorbed through an oxygen atom of the –CO group (due to its high negative electrostatic potential) onto carbon atoms surrounding the vacancy in SVG. The calculated adsorption energy in this configuration was substantial (Ead = -1.196 eV). NBO analysis indicated a minimal positive charge transfer (0.0073 e) from AFB1 to SVG, implying that AFB1 acts as an electron donor, while SVG functions as an electron acceptor in this complex. Figure 2.d also presents the

HOMO and LUMO profiles of the AFB1 molecule, the extent of these orbitals illustrates that the interaction likelihood is enhanced in the presence of functional groups. Since the molecular electrostatic potential (MEP) levels in the gas phase are the most important factors that affect the interaction between molecules, these levels were calculated for the AFB1 molecule [38]. As shown in Figure 1.d, the MEP maps reveal that oxygen atoms in AFB1 (particularly those in the –CO group) exhibit higher negative electrostatic potentials compared to carbon and hydrogen atoms. Consequently, these oxygen atoms have a greater propensity to bind to electron-deficient sites. Furthermore, among the studied configurations, S3 (E_{ad} = -1.196 eV) demonstrated higher stability than complexes S1 and S2, where adsorption occurred through the –OCH3 groups or the fouran ring structure onto the carbons surrounding the vacancy. As explained further in Figure 1.d, AFB1 molecules possess four nucleophilic sites: the –CO, –COO, –OCH3, and the two furan rings. The resonance of the double bonds of the two furan rings as well as the lone pairs of the oxygen atom in the –OCH3 group with the benzene rings significantly diminishes the nucleophilic character of these functional groups. Additionally, the lone pairs of the oxygen atom (sp^3) in the –COO group resonated with the –CO on one hand and with the benzene ring on the other hand, further reducing the interaction strength. Consequently, only the two oxygen atoms of the –CO groups, whose lone pairs do not participate in resonance, are capable of attacking the electron-deficient vacancy sites on SVG. This leads to the formation of the most stable complex, where the AFB1 molecule approaches the SVG surface via the oxygen atom of its carbonyl group (complex S3). This stabilization results in an increase in the energy gap from 0.54 eV to 0.88 eV and an augmentation of the hardness from 0.27 eV to 0.44 eV. These findings align with the observed high adsorption energy (-1.196 eV), indicative of strong chemical adsorption, as well as a reduction in the work function (from 3.53 eV to 3.42 eV).

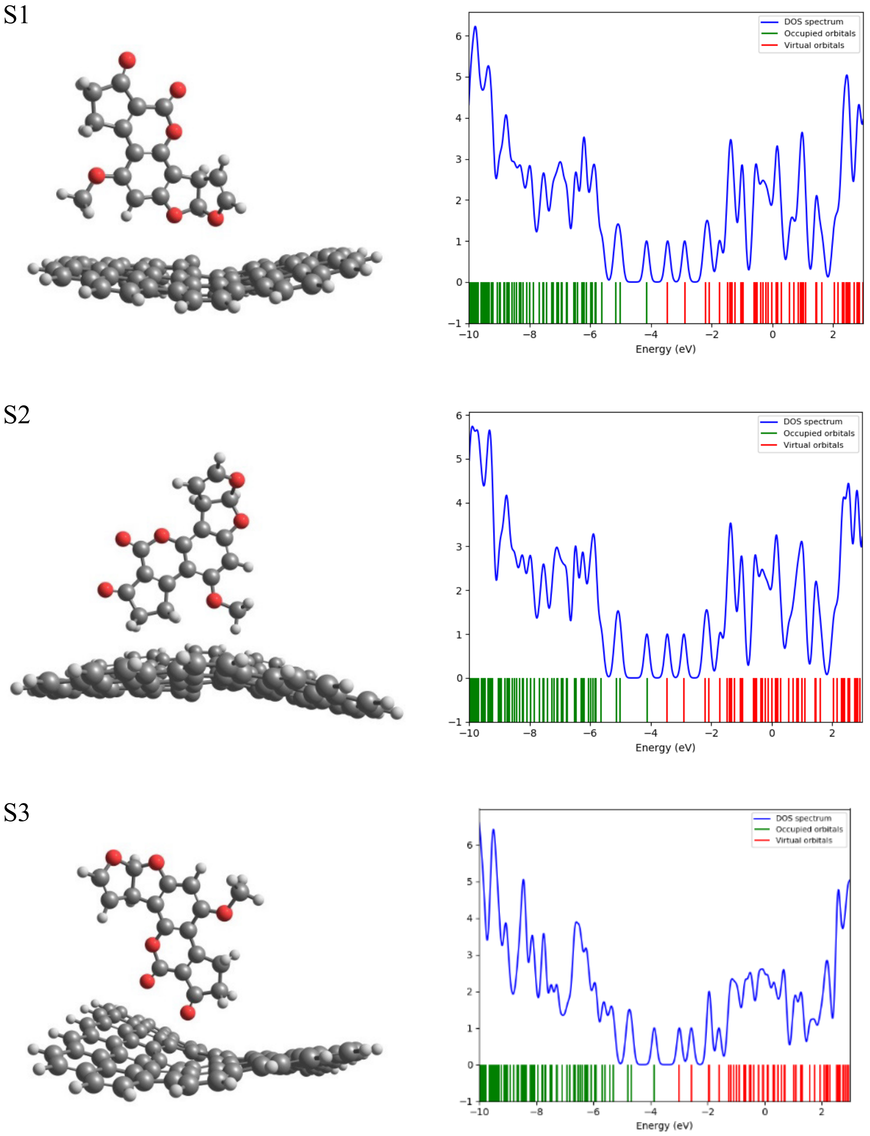

Fig. 3. Optimized structures and their DOS plot of AFB1/SVG complexes.

Moreover, in the S3 complex, the interaction between the antibonding orbitals of the –CO group and the LUMO orbital of SVG causes a destabilization of the LUMO energy level from -3.27 eV to -2.99 eV, while the HOMO energy level undergoes only minor changes (from -3.81 eV to -3.87 eV). These shifts in the energy levels of the frontier orbitals result in a 62% increase in the E_g, which, according to Equation 2, enhances the electrical conductivity and generates an electrical signal upon AFB1 detection. As detailed in Table 1, the AFB1 adsorption markedly reduces the work function from 3.54 eV to 3.43 eV, leading to an increased electron current density emitted by SVG in the presence of AFB1. This suggests that SVG nanosheets can function as efficient ϕ-type sensors for AFB1, acquiring a negative charge (electron transfer from AFB1 to SVG) during detection.

3.1.3. AFB1 adsorption onto graphene with double vacancy

The optimized structure of the graphene nanosheet with a double vacancy (DVG), along with its DOS spectra is illustrated in Figure 1. In the DVG model (Figure 2c), the HOMO band is delocalized throughout the carbon network, similar to PG. However, the LUMO band predominantly localizes on the eight carbon atoms surrounding the vacancy, with the highest electron density observed on the partially unsaturated carbon atoms within the five-membered rings. This spatial distribution, characterized by the expansion of the HOMO and LUMO molecular orbitals beyond bonds and atoms near the vacancy, explains why AFB1 adsorption on DVG is relatively weak. The maximum adsorption energy observed in configuration D3 was approximately -0.833 eV, which is insufficient to cause significant shifts in the energy levels of these molecular orbitals, with an observed percentage change in the energy gap of only 8.64%. As shown in Table 1, the introduction of a double vacancy increases the *Eg* from 0.81 eV (in PG) to 1.09 eV, and the hardness from 0.405 eV to 0.54 eV. These alterations indicate a reduction in the reactivity of DVG compared to PG. The optimized structures of AFB1/DVG and their corresponding DOS diagrams are presented in Fig. 2 Supp. in the supplementary file.

The relatively small $\%\Delta Eg$ values suggest that DVG is unlikely to function effectively as a ϕ-type sensor. The minimal change in the energy gap upon AFB1 adsorption indicates that the molecule's detection or sensing capability is limited. Although the Kohn–Sham band gap for some adsorbed configurations increases, the local density of states near the Fermi level reveals adsorbate-induced states that enhance charge transport channels. Thus, the macroscopic conductivity may increase despite a modest widening of the computed Eg. Additionally, the low adsorption energies imply that DVG cannot adsorb AFB1 strongly enough to be considered an effective sensor. As a result, DVG exhibits limited (or no) ability to detect AFB1.

3.2. AIM Analysis

The Atoms in Molecules (AIM) theory, introduced by Richard Bader, defines the chemical structure of a system based on the distribution of electron density between atoms [63]. Figure 4 depicts the molecular graphs for configurations S1, S2, and S3, illustrating the positions of all bond critical points (BCPs) between AFB1 and SVG. The presence of BCPs serves as evidence for chemical bonds formed between interacting atoms. Table 2 presents the calculated values of electron density ρ(r), the Laplacian $\nabla^2\rho$, as well as other properties such as kinetic energy density *G*, potential energy density *V*, total energy density *H*, and the ratio $\frac{|V(r)|}{G(r)}$. Higher positive values of $\nabla^2\rho$ and ρ(r) indicate stronger chemical bonds. Conversely, low charge density ρ(r) suggests that the interaction is primarily weak Van der Waals forces. When the signs of ρ(r) and *H* oppose each other, the bond exhibits partial covalent and electrostatic character. The ratio $\frac{|V(r)|}{G(r)}$ is a useful parameter for classifying the nature of interatomic interactions: Electrostatic interactions are associated with $\frac{|V(r)|}{G(r)} \leq 1$, intermediate interactions $1 < \frac{|V(r)|}{G(r)} < 2$, and the shared interactions $\frac{|V(r)|}{G(r)} > 2$ [64].

Table 2. AIM topological parameters at the bond critical points (BCPs) of the studied complexes, calculated using the B3LYP/6-31g(d) level of theory. All values are given in atomic units (a.u.)

Complex	BCP	$\rho(r)$	$\nabla^2\rho$	G	V	H	$\frac{\lvert V(r)\rvert}{G(r)}$	Interaction type
S1	p1	0.0039	0.0148	-0.0007	-0.0023	0.0007	0.0030	van der Waals
S1	p2	0.0037	0.0147	-0.0007	-0.0023	0.0007	0.0030	van der Waals
S1	p3	0.0028	0.0091	-0.0005	-0.0012	0.0005	0.0017	van der Waals
S1	p4	0.0022	0.0076	-0.0004	-0.0010	0.0004	0.0015	van der Waals
S1	p5	0.0025	0.0083	-0.0005	-0.0011	0.0005	0.0016	van der Waals
S2	p6	0.0042	0.0131	-0.0008	-0.0018	0.0008	0.0025	van der Waals
S3	p7	0.0006	0.0027	-0.0002	-0.0003	0.0002	0.0005	van der Waals
S3	p8	0.0008	0.0029	-0.0002	-0.0003	0.0002	0.0005	van der Waals
S3	p9	0.0051	0.0194	-0.0008	-0.0032	0.0008	0.0040	van der Waals
S3	p10	0.0014	0.0069	-0.0005	-0.0008	0.0005	0.0013	van der Waals

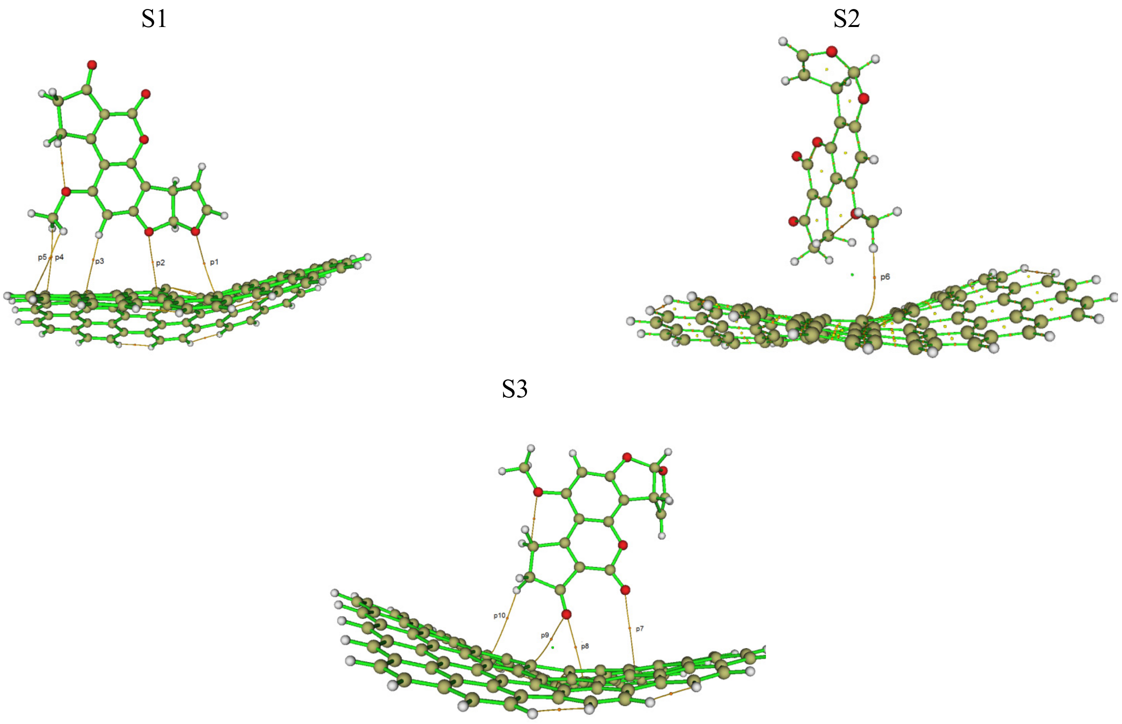

Fig. 4. The obtained molecular graphs of the AFB1/SVG complexes.

According to Table 2, the cases where $\frac{|V(r)|}{G(r)}$ is less than one, with both $\nabla^2\rho$ and H being positive or very low, and electron densities being minimal, indicate that the dominant interactions are of *Van der Waals* type. Although these are weak attractions, the presence of vacancies increases the local electron density, thereby enhancing adsorption properties and shifting the interaction from purely *Van der Waals* to electrostatic forces. This transition supports the observed increase in adsorption energy, corroborating the impact of vacancies on interaction strength.

4. Conclusion

This study employed DFT calculations to investigate the adsorption of AFB1 on PG, SVG and DVG. The results demonstrate that the presence of vacancies significantly enhances the adsorption capability of graphene, with SVG exhibiting superior performance compared to DVG and PG. The adsorption of AFB1 on SVG, particularly via the –CO oxygen atom near the vacancy site, leads to substantial binding, whereas PG shows weak interactions.

Electronic analyses including DOS, NBO, and AIM confirm that adsorption on SVG induces pronounced electronic modifications, such as a 62% reduction in the energy gap, lowering of the LUMO level, and decreased work function, collectively resulting in enhanced electrical conductivity and surface electron current density. In contrast, PG and DVG exhibit minimal electronic perturbations upon adsorption. AIM analysis further indicates that the interaction between AFB1 and SVG is predominantly physisorption, driven by *Van der Waals* forces. Overall, the findings highlight that the adsorption behavior and electronic properties of graphene–AFB1 complexes are strongly dependent on vacancy type and adsorption configuration. The remarkable electronic modulation observed in SVG underscores the critical role of defect engineering in optimizing graphene-based nanosensors, establishing single-vacancy graphene as a highly promising platform for sensitive AFB1 detection. In the continuation of this research, future efforts will focus on a comprehensive experimental validation of the predicted sensing behavior. Time-resolved adsorption and desorption measurements will be performed to investigate the dynamic aspects of the sensing process, while spectroscopic characterization will be employed to confirm charge-transfer and binding interactions between the target molecule and the graphene surface.

To account for entropic and environmental effects, explicit-solvent molecular dynamics simulations will be conducted under various pH and temperature conditions. From a theoretical standpoint, free-energy and desorption barrier calculations will be carried out to provide a more accurate description of adsorption thermodynamics and kinetics. Furthermore, various graphene functionalization strategies such as doping and surface chemical modification will be explored to enhance the selectivity and sensitivity toward AFB1. Finally, device-level modeling and simulation will be undertaken to bridge molecular-scale predictions with macroscopic sensor performance, paving the way for the rational design of next-generation sensing devices.

Supplementary files

Supplementary file 1.

References

[1] C. F. Jelinek, A. E. Pohland, G. E. Wood, Review of mycotoxin contamination. Worldwide occurrence of mycotoxins in foods and feeds—an update. *J. Assoc. Anal. Chem.*, 72 (1989) 223–230.

[2] K. K. Sinha, Incidence of mycotoxins in maize grains in Bihar State, India. *Food Addit. Contam.*, 7 (1990) 55–61.

[3] K. K. Sinha, *Mycotoxin Induced Abnormalities in Crop Plants*. M.D. Publications Private, New Delhi (1996).

[4] L. Romani, Immunity to fungal infections. *Nat. Rev. Immunol.*, 4 (2004) 1–23.

[5] V. Moudgil, D. Redhu, S. Dhanda, J. Singh, A review of molecular mechanisms in the development of hepatocellular carcinoma by aflatoxin and hepatitis B and C viruses. *J. Environ. Pathol. Toxicol. Oncol.*, 32 (2013) 165–175.

[6] Testing methods for aflatoxins in foods. *Food Nutr. Bull.*, 20 (1999) 458-464.

[7] J. Gao, S. He, A. Nag, J. Woon, C. Wong, A review of the use of carbon nanotubes and graphene-based sensors for the detection of aflatoxin M1 compounds in milk. *Sensors*, 21 (2021) 3602.

[8] M. Koohi, H. Bastami, A quest for stable 2,2,9,9-tetrahaloplumbacyclonona-3,5,7-trienylidenes at density functional theory. *Struct. Chem.*, 31 (2020) 877-898.

[9] C. Berger, Z. Song, T. Li, X. Li, A. Ogbazghi, R. Feng, et al., Ultrathin epitaxial graphite: 2D electron gas properties and a route toward graphene-based nanoelectronics. *J. Phys. Chem. B*, 108 (2004) 19912–19916.

[10] M. Koohi, H. Bastami, Investigation of Ti—B nanoheterofullerenes evolved from C_{20} nanocage through DFT. *Chem. Rev. Lett.*, 6 (2023) 223-234.

[11] R. Rahman-Abadi, M. Haghgu, Z. Rostami, R. Behjatmanesh-Ardakani, Investigating the role of transition metals of Zn, Fe and Cu and the basis of single and double-cavity defective graphenes in the regeneration of CO_2 gas. *Mol. Phys.*, 122 (2024) 2341107.

[12] A. H. Castro Neto, F. Guinea, N. M. R. Peres, K. S. Novoselov, A. K. Geim, The electronic properties of graphene. *Rev. Mod. Phys.*, 81 (2009) 109–162.

[13] S. Esfahani, J. Akbari, S. Soleimani-Amiri, Adsorption of ibuprofen by an iron-doped silicon carbide graphene monolayer: DFT exploration of drug delivery insights. *Int. J. Nano Dimens.*, 15 (2024) 63-71.

[14] S. J. Hoseyni, A. Karbakhshzadeh, A. Moshtaghi Zonouz, B. Husseen, Computational investigation on interaction between graphene nanostructure BC_3 and antiparkinson drug amantadine: Possible sensing study of BC_3 and its doped derivatives on amantadine. *Chem. Rev. Lett.*, 7 (2024) 380-387.

[15] E. Vessally, M. R. Ilghami, M. Abbasian, Investigation the capability of doped graphene nanostructure in magnesium and barium batteries with quantum calculations. *Chem. Res. Technol.*, 1 (2024) 204–211. https://doi.org/10.2234/chemrestec.2024.436837.1007

[16] T. Yadollahi, R. Ghiasi, S. Baniyaghoob, Unveiling of interactions of ansa-titanocene dichloride and ansa-vanadocene dichloride anticancer drugs with $B_{12}N_{12}$ cage. *Inorg. Chem. Commun.*, 173 (2025) 113896.

[17] R. Ghiasi, M. Nikbakht, H. Pasdar, Interactions of the potential antitumor agent vanadocene dichloride with C_{20} and $M^+@C_{20}$ (M= Li, Na, K) nano-cages: A DFT investigation. *Results Chem.*, 9 (2024) 101659.

[18] R. Ghiasi, M. Nikbakht, A. Amiri, Understanding the interactions between anticancer active molecules Cp_2TiCl_2 and Cp_2VCl_2 and $E@Al_{12}$ (E=C, Si) cluster using Density Functional Theory calculations. *Inorg. Chem. Commun.*, 164 (2024) 112446.

[19] R. Behjatmanesh-Ardakani, R. Rzayev, Hydrogen assisted SO_2 dissociation on the Pt-doped graphene quantum dot surface: a non-periodic DFT study. *Chem. Rev. Lett.*, 8 (2025) 178-186.

[20] A. Solgi, R. Ghiasi, S. Baniyaghoob, PCM, ETS-NOCV, and CDA investigations of interactions of a cycloplatinated thiosemicarbazone as antiparasitic and antitumor agents with C_{20} nano-cage. *Int. J. Nano Dimens.*, 14 (2023) 219-226.

[21] R. Ghiasi, A. Valizadeh, Computational investigation of interaction of a cycloplatinated thiosemicarbazone as antitumor and antiparasitic agents with $B_{12}N_{12}$ nano-cage. *Results Chem.*, 5 (2023) 100768.

[22] M. Shabani, R. Ghiasi, R. Fazaeli, Computational investigation of interaction between titanocene dichloride and nanoclusters ($B_{12}N_{12}$, $B_{12}P_{12}$, $Al_{12}N_{12}$ and $Al_{12}P_{12}$). *Main Group Chem.*, 20 (2021) 437-444.

[23] F. Banhart, J. Kotakoski, A. V. Krasheninnikov, Structural defects in graphene. *ACS Nano*, 5 (2011) 26-41.

[24] S. N. Adawara, A. S. Isa, F. A. Yaro, M. A. Tijjani, U. T. Mamza, M. Iji, et al., Triazolopyrimidine derivatives for cancer: An in silico evaluation of docking and pharmacokinetics. *J. Chem. Technol.*, 1 (2025) 116–125. https://doi.org/10.22034/jchemtech.2025.539505.1016.

[25] F. Najafi, S. S. Alamdar, E. Vaziri, Fullerene (C_{20}) as a sensor for the detection of nordazepam: DFT simulations. *J. Med. Med. Chem.*, 1 (2025) 18–23. https://doi.org/10.22034/jmedchem.2025.526412.1004.

[26] S. A. Vahed, $B_{12}N_{12}$ as a sensor for the detection of nordazepam. *J. Med. Med. Chem.*, 1 (2024) 14–19. https://doi.org/10.22034/medmedchem.2024.474845.1008.

[27] M. R. Jalali Sarvestani, Potentiometric sensors developed for the measurement of pharmaceutical compounds. *J. Med. Med. Chem.*, 1 (2024) 84–90. https://doi.org/10.22034/medmedchem.2024.475078.1010.

[28] Z. Jabarzadeh, M. R. Jalali Sarvestani, S. Arabi, M. Mahboubi-Rabbani, Sh. Ahmadi, A potentiometric sensor for highly selective and sensitive determination of flurazepam in pharmaceutical and biological samples based on molecularly imprinted polyaniline as the ionophore. *J. Chem. Lett.*, 8 (2025) 576-588.

[29] S. Hessen, N. M. A. Alsultany, H. Bahir, A. Husein Adthab, S. Soleimani-Amiri, Sh. Ahmadi, et al., Adsorption of sulfur mustard on the transition metals (TM = Ti^{2+}, Cr^{2+}, Fe^{2+}, Co^{2+}, Ni^{2+}, Cu^{2+}, Zn^{2+}) porphyrins induced in carbon nanocone (TM-PCNC): Insight from DFT calculation. *J. Mol. Graph. Model.*, 135 (2025) 108928.

[30] M. W. Schmidt, K. K. Baldridge, J. A. Boatz, S. T. Elbert, M. S. Gordon, J. H. Jensen, et al., General atomic and molecular electronic structure system. *J. Comput. Chem.*, 14 (1993) 1347–1363.

[31] A. D. Becke, Density-functional thermochemistry. III. The role of exact exchange. *J. Chem. Phys.*, 98 (1993) 5648–5652.

[32] C. Lee, W. Yang, R. G. Parr, Development of the Colle-Salvetti correlation-energy formula into a functional of the electron density. *Phys. Rev. B*, 37 (1988) 785–789.

[33] B. Civalleri, C. M. Zicovich-Wilson, L. Valenzano, P. Ugliengo, B3LYP augmented with an empirical dispersion term (B3LYP-D*) as applied to molecular crystals. *CrystEngComm*, 10 (2008) 405–410.

[34] S. Grimme, Accurate description of van der Waals complexes by density functional theory including empirical corrections. *J. Comput. Chem.*, 25 (2004) 1463–1473.

[35] M. Abosaooda, H. Bahir, N. Ali Salman, S. Kamil Abbood, L. Yassen Qassem, I. A. Kadhim Jassem, et al., Evaluate the potential utilisation of B_3S monolayer as a novel formaldehyde gas sensor. *Mol. Phys.*, 122 (2023) 2294154.

[36] Z. Rostami, M. Maskanati, S. Khanahmadzadeh, M. Dodangi, M. Nouraliei, Interaction of nitrotyrosine with aluminum nitride nanostructures: A density functional approach. *Physica E*, 116 (2020) 113735.

[37] M. R. Poor Heravi, B. Azizi, E. A. Mahmood, A. Gh. Ebadi, M. J. Ansari, S. Soleimani-Amiri, Molecular simulation of the paracetamol drug interaction with Pt-decorated BC_3 graphene-like nanosheet. *Mol. Simul.*, 48 (2022) 517-525.

[38] Z. Rostami, M. Asnaashariisfahani, Sh. Ahmadi, A. Hosseinian, A. Ebadi, A density functional theory investigation on 1H-4-germapyridine-4-ylidene & the unsaturated heterocyclic substituted ones. *J. Mol. Struct.*, 1238 (2021) 130427.

[39] N. Mirderikvand, M. Mahboubi-Rabbani, A DFT study on citalopram adsorption on the surface of $B_{12}N_{12}$. *J. Chem. Technol.*, 1 (2025) 90–95. https://doi.org/10.22034/jchemtech.2025.538393.1015.

[40] N. O'Boyle, A. Tenderholt, K. Langner, A library for package-independent computational chemistry algorithms. *J. Comput. Chem.*, 29 (2008) 839–845.

[41] K. R. Hossain, M. M. A. Shishir, S. Rashid, M. H. Ahmed, A. Basher, R. H. Risad, et al., Application of 3D printing technology in the military. *J. Chem. Lett.*, 4 (2023) 103–116.

[42] S. F. Boys, F. Bernardi, The calculation of small molecular interactions by the differences of separate total energies. Some procedures with reduced errors. *Mol. Phys.*, 19 (1970) 553–561.

[43] A. Pulido, M. Boronat, A. Corma, Theoretical investigation of gold clusters supported on graphene sheets. *New J. Chem.*, 35 (2011) 2153–2161.

[44] E. Kaxiras, K. C. Pandey, Energetics of defects and diffusion mechanisms in graphite. *Phys. Rev. Lett.*, 61 (1988) 2693–2696.

[45] A. A. El-Barbary, R. H. Telling, C. P. Ewels, M. I. Heggie, P. R. Briddon, Structure and energetics of the vacancy in graphite. *Phys. Rev. B*, 68 (2003) 144107.

[46] P. O. Lehtinen, A. S. Foster, Y. Ma, A. V. Krasheninnikov, R. M. Nieminen, Irradiation-induced magnetism in graphite: A density functional study. *Phys. Rev. Lett.*, 93 (2004) 187202.

[47] Y. Ma, P. O. Lehtinen, A. S. Foster, R. M. Nieminen, Magnetic properties of vacancies in graphene and single-walled carbon nanotubes. *New J. Phys.*, 6 (2004) 68.

[48] R. Behjatmanesh-Ardakani, H. Mohammadi-Manesh, M. Sedaghatjou, Pt-embedded pyrrolic and pyridinic N-doped graphene quantum dots as a viable aflatoxin B1 sensor: Insights from DFT calculations. *Chem. Rev. Lett.*, (2025) *in press*.

[49] R. L. Hsian, V. K. Hussin, O. A. Hamad, R. O. Kareem, Theoretical study chlorohydroquinone with substituted lithium via quantum computation methods. *Chem. Res. Technol.*, 1 (2024) 73–77. https://doi.org/10.2234/chemrestec.2024.448968.1009.

[50] F. Iorhuna, A. M. Ayuba, A. T. Nyijime, Comparative study of skimmianine as an adsorptive inhibitor on Al(110) and Fe(111) crystal surface, using DFT and simulation method. *J. Chem. Lett.*, 4 (2023) 148–155. https://doi.org/10.22034/jchemlett.2023.398506.1117.

[51] R. Ahmadi, Furazolidone adsorption on the surface of $B_{12}N_{12}$: DFT simulations. *J. Med. Med. Chem.*, 1 (2025) 100–105. https://doi.org/10.22034/jmedchem.2025.547065.1018.

[52] I. Baikie, S. Mackenzie, P. Estrup, J. A. Meyer, A study of the electronic properties of graphite and related materials. *Rev. Sci. Instrum.*, 62 (1991) 1326–1332.

[53] S. A. Sangam, R. P. Bakale, M. Gumaste, S. N. Mathad, S. Desai Desai, Advances in biosensors: A comprehensive review of types, enzyme-based glucose biosensors, and applications. *J. Chem. Lett.*, 6 (2025) 33–48. https://doi.org/10.22034/jchemlett.2024.472796.1220.

[54] L. Saedi, Z. Rostami, B. Rabiei, N. Othman Kattab, M. Volek, X. Hong, Identification of lomustine drug by graphyne-like boron nitride: DFT approach. *Mol. Phys.*, (2024) e2318022.

[55] O. Richardson, The absorption of X-rays by gases. *Phys. Rev.*, 23 (1924) 153–155.

[56] F. Banhart, J. Kotakoski, A. V. Krasheninnikov, Structural defects in graphene. *ACS Nano*, 5 (2011) 26–41.

[57] S. A. Vahed, Fullerene (C_{20}) as a sensor for detection of midazolam: Theoretical insights. *J. Med. Med. Chem.*, 1 (2025) 106–110. https://doi.org/10.22034/jmedchem.2025.547513.1019.

[58] I. A. Pašti, A. Jovanović, A. S. Dobrota, S. V. Mentus, B. Johansson, N. V. Skorodumova, Atomic adsorption on pristine graphene along the periodic table of elements from PBE to non-local functionals. *Appl. Surf. Sci.*, 436 (2017) 433–440.

[59] A. V. Krasheninnikov, P. O. Lehtinen, A. S. Foster, R. M. Nieminen, Defects in graphene: The vacancy. *Chem. Phys. Lett.*, 418 (2006) 132–136.

[60] A. A. El-Barbary, R. H. Telling, C. P. Ewels, M. I. Heggie, P. R. Briddon, Structure and energetics of the vacancy in graphite. *Phys. Rev. B*, 68 (2003) 144107.

[61] A. H. Nevidomskyy, G. Csányi, M. C. Payne, Chemically active substitutional nitrogen impurity in carbon nanotubes. *Phys. Rev. Lett.*, 91 (2003) 105502.

[62] A. V. Krasheninnikov, P. O. Lehtinen, A. S. Foster, P. Pyykkö, R. M. Nieminen, Embedding transition-metal atoms in graphene: Structure, bonding, and magnetism. *Phys. Rev. Lett.*, 102 (2009) 126807.

[63] P. Shyam Vinod Kumar, V. Raghavendra, V. Subramanian, Bader's theory of atoms in molecules (AIM) and its applications to chemical bonding. *J. Chem. Sci.*, 128 (2016) 1527–1536.

[64] D. V. Korabel'nikov, Y. N. Zhuravlev, The nature of the chemical bond in oxyanionic crystals based on QTAIM topological analysis of electron densities. *RSC Adv.*, 9 (2019) 12020–12033.